Geochemical Perspectives Letters

Pyrite-based trace element fingerprints for methane and oil seepage

D. Smrzka[1,2*], Z. Lin[3], P. Monien[2], T. Chen[4], W. Bach[1,2], J. Peckmann[3], G. Bohrmann[1,2]

https://doi.org/10.7185/geochemlet.2409

Abstract

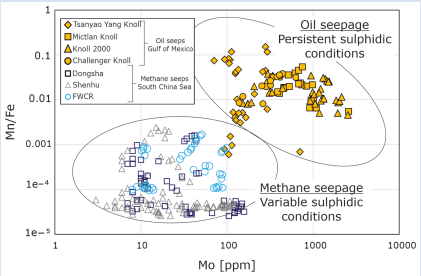

Pyrite forms at marine hydrocarbon seeps as the result of the microbial oxidation of methane, organic matter, and crude oil coupled to sulphate reduction. Redox sensitive and nutrient trace elements in pyrite may hold valuable information on present and past seepage events, the evolution of fluid composition, as well as the presence of heavy hydrocarbon compounds from crude oil. This study uses the trace element compositions of pyrite that formed at methane seeps and crude oil-dominated seeps to constrain element mobilities during the sulphate reduction processes, and examine the degree to which specific trace elements are captured by pyrite. Pyrite forming at oil seeps shows high Mn/Fe ratios and high Mo content compared to pyrite from methane seeps. These patterns suggest either more intense or persistent sulphidic conditions, or an intensified manganese (oxy)hydroxide shuttle process at oil seeps. Copper and Zn are enriched in oil seepage-derived pyrite while Ni and V enrichment is less pronounced, suggesting either a selective uptake of specific elements by pyrite, or varying trace element compositions of organic compounds oxidised *via* microbial reduction.

Received 24 September 2023 | Accepted 30 January 2024 | Published 5 March 2024

Introduction

Marine hydrocarbon seeps support chemosynthesis-based microbial habitats of archaea and sulphate reducing bacteria performing the sulphate driven anaerobic oxidation of methane (SD-AOM). This process triggers the formation of authigenic minerals that record the dynamics and intensity of seepage, redox fluctuations, and the evolution of fluid composition and microbial activity (Feng *et al.*, 2009; Smrzka *et al.*, 2016, 2019a). Pyrite is a widespread mineral that forms during sulphate reduction at seeps, which are hotspots of pyrite authigenesis. Detailed studies on pyrite morphology and its stable isotopic and trace element compositions have recently been conducted in seep settings (Lin *et al.* 2022; Wang *et al.*, 2022).

Pyrites from various environments show different trace element patterns depending on morphology, grain size, formation temperatures, and the composition of parent fluids (Gregory *et al.*, 2015). The trace element inventory of pyrite has been refined into a first order proxy for the deep time evolution of Earth's biosphere (Large *et al.*, 2014). Sedimentary pyrite formation is controlled by the biogeochemical cycles of sulphur, carbon and iron, and constitutes a relevant long term sink for trace elements during early diagenesis (Huerta-Diaz and Morse, 1992). Pyrite scavenges and incorporates trace elements from parent fluids, including many redox sensitive and bio-essential trace metals including Mn, Mo, Ni, Cu, Zn, Cr, As and Se (Huerta-Diaz and Morse, 1992; Morse and Arakaki, 1993). Pyrite based proxies for fluid composition, sulphate reduction processes and redox conditions are a trending topic in hydrocarbon seep research (Miao *et al.*, 2022, Lin *et al.*, 2022; Wang *et al.*, 2022; Domingos *et al.*, 2023). Hydrocarbon emissions from natural methane and oil seeps represent prominent pathways of carbon transfer from the geosphere to the hydrosphere. Constraining their influence on the marine carbon and sulphur cycles is therefore critical in order to improve the quantification of global methane budgets and to understand the dynamics of – and responses to – natural and anthropogenic oil spills. A pyrite based proxy offers insights into the evolution of fluid composition at seeps, which is critical because fluid composition governs microbial and metazoan ecology (Orcutt *et al.*, 2010). The significance of distinguishing oil- from methane-dominated seep systems has gained traction in recent years in the search for end member system identification (Smrzka *et al.*, 2016; Akam *et al.*, 2021; Krake *et al.*, 2022), and reliable proxies are continuously being explored and refined.

This study presents a first comparison of the trace element compositions of authigenic pyrite derived from methane and oil seeps. Motivated by current efforts to exploit the potential of pyrite based geochemical proxies, we provide new constraints on environmental conditions during seepage and microbial oxidation of heavy hydrocarbons, and establish trace element fingerprints to distinguish methane seeps from oil dominated seeps. These results improve our understanding of trace element

1. MARUM Zentrum für Marine Umweltwissenschaften, 28359 Bremen, Germany
2. Fachbereich Geowissenschaften, Universität Bremen, 28359 Bremen, Germany
3. Institut für Geologie, Centrum für Erdsystemforschung und Nachhaltigkeit, Universität Hamburg, 20146 Hamburg, Germany
4. CAS Key Laboratory of Crust-Mantle Materials and Environments, School of Earth and Space Sciences, University of Science and Technology of China, Hefei 230026, China
* Corresponding author (email: dsmrzka@marum.de)

liberation during microbial sulphate reduction, and their subsequent incorporation into pyrite during early diagenesis, while emphasising the role of pyrite based trace element geochemistry as a main, or complementary, source of information on redox conditions and fluid compositions in modern, and potentially, ancient seepage environments.

Study Sites – Endmembers of Hydrocarbon Seepage

Two localities of methane and heavy hydrocarbon seepage were selected for a comparative study of authigenic pyrite forming in different environments. The Campeche and Sigsbee Knolls in the southern Gulf of Mexico (GoM; Fig. 1a) are two salt provinces that exhibit a set of hummocky seafloor structures related to salt tectonism, enabling the seepage of methane and crude oil, as well as the formation of gas hydrates within the sediments and on the seafloor (Sahling *et al.*, 2016). Crude oil and asphalt in the southern GoM fuel microbial sulphate reduction independent of SD-AOM (Joye *et al.*, 2004), and have shaped a unique environment inhabited by distinct macro- and micro-faunal communities (Orcutt *et al.*, 2010). This study considers the Campeche and Sigsbee Knolls as crude oil dominated end member seepage systems.

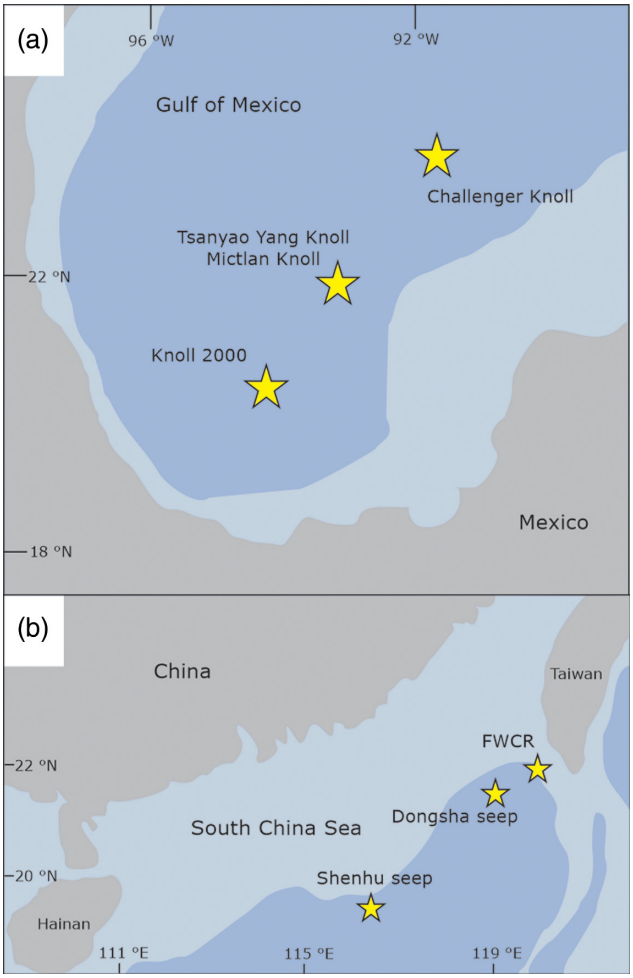

Figure 1 Locations of the investigated sediment cores. **(a)** Gravity core locations from oil seeps at Campeche and Sigsbee Knolls in the southern Gulf of Mexico. **(b)** Gravity core locations of methane seeps from the South China Sea.

The South China Sea (SCS) is a large marginal sea in the western Pacific Ocean located at the transect between the Eurasian, Pacific, and Indian plates (Fig. 1b). The northern SCS is a passive continental margin covered by thick successions of Neogene sediments that promote abundant hydrocarbon generation manifested as mud volcanoes and diapirs, gas chimneys, and seafloor seepage sites. Among the numerous seep sites discovered in the SCS over the past decades, the Dongsha and Shenhu seepage provinces are among the best studied sites, which have been previously studied regarding the genesis of authigenic pyrite (Lin *et al.*, 2022). To the northeast of these seepage areas, and related to the convergence of the Eurasian and the Philippine Sea plates, lies the south-western Taiwan accretionary prism, which harbours the Yam Seep area located at the northern crest of Four-Way Closure Ridge (FWCR; Tseng *et al.*, 2023). The Dongsha, Shenhu, and Yam Seep sites are all characterised by seepage of biogenic and thermogenic methane, representing methane dominated end member seepage systems.

Material and Methods

Authigenic pyrite was obtained from a total of five gravity cores, which were sampled over the course of four cruises between 2015 and 2018 in the southern GoM and the northern SCS (Fig. 1). Between 20 and 30 grams of sediment were sampled from the cores at intervals of 20 cm, freeze dried over 24 hrs, and subsequently powdered by hand using an agate pestle and mortar. Aliquots of unpowdered sediment were then sieved with deionised water through a 0.063 mm sieve, and pyrite aggregates were hand picked under a binocular microscope from the coarse fraction. Pyrite grains were mounted onto epoxy discs, polished to a smooth surface and coated with carbon for scanning electron microscopy and electron probe microanalysis (EMPA). Major element content in pyrite was determined using a Cameca SX-100 electron microprobe. Major and trace element composition of pyrite was determined *via* laser ablation inductively coupled plasma mass spectrometry (LA-ICP-MS). All element data and additional information are given in the Supplementary Information.

Results

Manganese, Mo, Cu, and Zn contents in pyrite show different distribution patterns for the two investigated types of hydrocarbon seepage. Pyrite from oil dominated seeps is characterised by higher content of Mn and Mo than in methane seepage-derived pyrite. The Mn enrichment is expressed as Mn/Fe ratios shown in Figure 2, which is two to three orders of magnitude higher in oil seepage-derived pyrite. Molybdenum content is higher by one order of magnitude in oil seep pyrite (Fig. 2). Methane seep pyrite from the four sites shows variable Mn/Fe ratios. The contents of Cu and Zn are higher in oil seep pyrite than in methane seep pyrite, and the distribution of these elements allows for a distinction between the two seepage environments (Fig. 3a). This distinction is less clear for Ni and V (Fig. 3b).

Discussion

A combined Fe-Mn-Mo fingerprint. Microbial sulphate reduction at seeps is coupled to the oxidation of methane, sedimentary organic matter, and high molecular weight hydrocarbons that make up crude oil (Joye *et al.*, 2004; Smrzka *et al.*, 2019a). The microbial oxidation rates of these compounds are governed by the microbial consortium capable of using the particular electron donors, which affects sulphate reduction rates and thus the

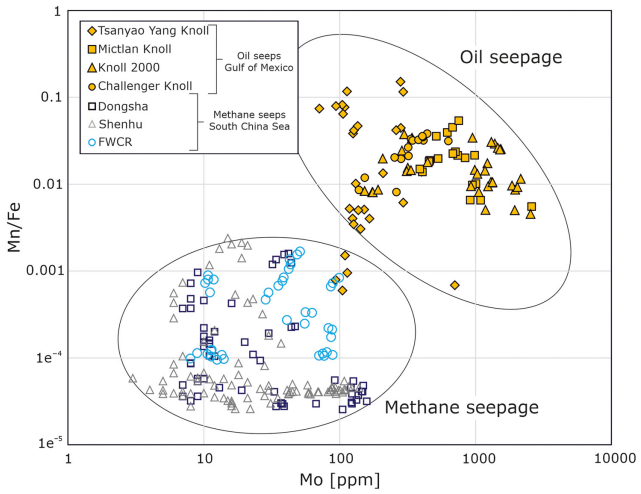

Figure 2 Mn/Fe ratios and Mo content in methane seepage- and oil seepage-derived authigenic pyrite. Data from Dongsha and Shenhu seepage areas are from Lin *et al.* (2022).

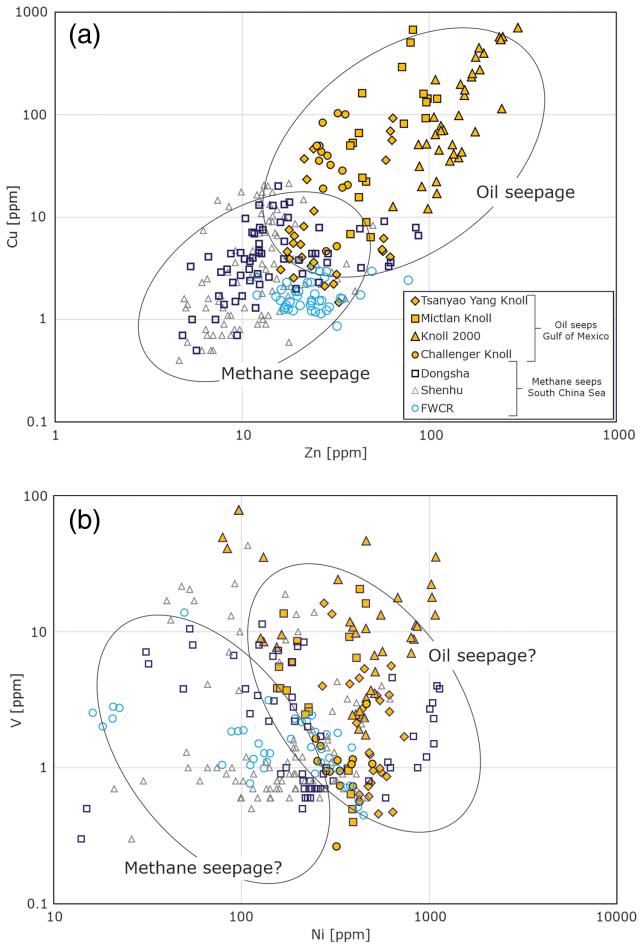

Figure 3 Trace element content in methane seepage- and oil seepage-derived authigenic pyrite. **(a)** Zn and Cu content, **(b)** Ni and V content; data from Dongsha and Shenhu seepage areas are from Lin *et al.* (2022).

amount of sulphide released to sedimentary pore water (Smrzka *et al.*, 2019a). The concentration of dissolved sulphide species in pore fluids in turn influences the solubility and mobility of redox sensitive trace elements, particularly Mo and to a lesser extent Mn. In addition, the oxidation of sedimentary organic matter and crude oil will inevitably lead to the partial or complete breakdown of organic compounds, which are themselves carriers of trace elements (Smrzka *et al.*, 2020).

Manganese and Mo contents in pyrite allow us to distinguish between the two seepage environments (Fig. 2). The Mo content in oil seep pyrite is up to an order of magnitude higher than in methane seep pyrite and sedimentary pyrite reported from black shales (Gregory *et al.*, 2015). Molybdenum is incorporated into pyrite under sulphidic conditions, after stabilising as thiomolybdate, and may also be fixed by organic matter (Morse and Luther, 1999; Gregory *et al.*, 2015). Manganese does not usually reside in pyrite in high concentrations, yet may form sulphides adsorbed to mackinawite; a precursor mineral of pyrite during early diagenesis (Gregory *et al.*, 2015). Manganese is usually incorporated into Ca-rich rhodochrosite or high-Mg calcite under sulphidic conditions during early diagenesis (Suess, 1978), but may incorporate into pyrite at high Mn^{2+} concentrations (Morse and Arakaki, 1993; Morse and Luther, 1999). Manganese incorporation into pyrite may also proceed *via* the uptake of precursor manganese sulphide phases, which are stable at high Mn/Fe ratios and high sulphide levels (Shikazono *et al.*, 1994). A recent study indicates that Mn is distributed randomly within pyrite and held within microcrystals that formed early during diagenesis, suggesting that the partitioning behaviour of dissolved Mn into authigenic minerals is not as straightforward as previously thought (Atienza *et al.*, 2023). Although Mn can be enriched in pyrite formed by SD-AOM (Lin *et al.*, 2022), the Mn/Fe ratios in pyrite from oil seeps are orders of magnitude higher than in pyrite from methane seeps (Fig. 2). High levels of dissolved sulphide favour the incorporation of Mn and Mo into pyrite (Wang *et al.*, 2022), suggesting that the microbial oxidation of crude oil in sediments may enable persistent and highly sulphidic conditions in ambient pore waters controlled by the extent and rate of microbial metabolism. Microbial crude oil oxidation coupled to sulphate reduction enables carbonate precipitation and sulphide production, despite its generally slower microbial oxidation rate compared to SD-AOM (Joye *et al.*, 2004; Smrzka *et al.*, 2019a). Components of crude oils contain variable contents of organic sulphur residing in compounds including thiols, sulphides, and thiophenes (Tissot and Welte, 1984). The high sulphur content in oils (>2 wt. %) from the southern GoM and the increase of dissolved hydrogen sulphide gas emitted at oil seeps (Smrzka *et al.*, 2019a) suggest that the microbial mineralisation of crude oil may act as an additional source of sulphur to pore waters.

The high Mn/Fe ratios of oil seep pyrite may also be due to an effective manganese (oxy)hydroxide shuttle process, transferring adsorbed trace elements from seawater to the sediments (Scholz *et al.*, 2013; Smrzka *et al.*, 2020). This shuttle may be intensified by the seepage of crude oil, acting as an additional source of Mn from sedimentary pore waters to bottom waters. Oil seeps at the Campeche Knolls emit oil droplets, oily gas bubbles, and asphalt fragments (Sahling *et al.*, 2016), which could act as an additional transport agent for trace elements to bottom waters. The emitted oil components will be oxidised aerobically in the bottom waters around the locus of seepage, releasing adsorbed or incorporated trace elements from organic compounds. This oil enhanced manganese (oxy)hydroxide shuttle would also explain the observed co-enrichment of Mn and Mo (*cf.* Scholz *et al.*, 2013) and to a lesser extent Cu (Fig. 3a) in oil seep pyrite.

A combined Cu-Zn-Ni-V fingerprint. Copper and Zn are commonly co-enriched in marine organic matter and seafloor sediments, yet they are taken up into pyrite to different degrees. Copper forms strong complexes with organic matter and

precipitates as copper sulphide during sulphate reduction (Morse and Luther, 1999). Copper enrichment in oil seep pyrite is likely derived from two sources, either released by reductive dissolution of manganese (oxy)hydroxides leading to a co-enrichment of Mn and Cu (Figs. 2, 3a) and released directly from crude oil during its microbial mineralisation. The affinity for Zn incorporation into pyrite is lower than for Cu due to ZnS precipitation prior to pyrite formation (Morse and Luther, 1999). Zinc content varies considerably in diagenetic pyrite where it may be present as sphalerite inclusions (Gregory *et al.*, 2015). However, both Zn and Cu are co-enriched in oil seep pyrite, suggesting an overriding effect of microbial crude oil oxidation coupled to sulphate reduction. Nickel and V are micronutrients for phytoplankton growth, and are transported to the seafloor by organic particles and metal (oxy)hydroxides (Smrzka *et al.*, 2019b). While Ni is commonly divalent in marine sediments, V is sensitive toward pH, redox conditions and dissolved sulphide concentrations, and V enrichment in reducing sediments relative to average continental crust (Thomson *et al.*, 1998). Whereas Ni is incorporated into pyrite during early diagenesis, V usually resides in the non-sulphide fraction such as organic matter, silicates and carbonates (Huerta-Diaz and Morse, 1992; Gregory *et al.*, 2015). In contrast to Cu and Zn, the distribution of Ni and V show large overlap without clear enrichments between methane and oil seep pyrite (Fig. 3b).

The release of trace elements during organic matter oxidation represents a source of trace elements during early diagenesis (Smrzka *et al.*, 2020), reflected by the trace element composition of pyrite (Miao *et al.*, 2022; Chen *et al.*, 2023). The present data set expands this distinction regarding the presence of oil compounds and their microbial mineralisation in marine sediments. Crude oils contain trace elements including Ni, V, Cu, and Zn, which are present as metalloporphyrin complexes derived from bacterial and plant pigments, as metal centres of microbial enzymatic cofactors, and in large organic matrices or other metal-binding functional groups (Duyck *et al.*, 2007). Only Cu and Zn are systematically enriched in oil seep pyrite relative to its methane seep counterpart. These distribution patterns may be controlled by differences in the incorporation behaviour of the respective element into the pyrite structure (Gregory *et al.*, 2015), the trace element composition of the oxidised organic compounds, the varying rates of microbial oil degradation, and the composition of the host sediment (Figure S-2) during pyrite formation.

Nickel and V reside in crude oils primarily as petroporphyrin complexes that are primarily part of the asphaltene fraction (Duyck *et al.*, 2007). Petroleum hydrocarbons from southern GoM seeps are biodegraded, weathered (Schubotz *et al.*, 2011) and of low thermal maturity with Zn, Cu and Ni content between 10 and 100 ppm, and V content of up to 400 ppm (Smrzka *et al.*, 2019a). The lack of V enrichment in oil seep pyrite is most likely due to its low affinity towards pyrite incorporation, which is lower than for other trace metals (Gregory *et al.*, 2015). Although a slight Ni enrichment in oil seep pyrite is present, it cannot be used as an unambiguous indicator for microbial crude oil mineralisation. Manganese (oxy)hydroxides are also effective transport agents for Ni and V to sediments (Smrzka *et al.*, 2019b), yet contrary to Mn and Mo, they are not distinctly enriched in oil seep pyrite. Also, the degree to which Ni and V are released from organic matter during microbial remineralisation may be smaller than for Cu and Zn. For instance, although all four elements reside in metalloporphyrins of organic matter and oils, biodegradation of nickel porphyrins is slower than for copper and vanadyl porphyrins (Sadowski *et al.*, 2007). Microbial mineralisation of crude oil, which occurs both anaerobically in the sediments and aerobically in bottom waters, may selectively release trace elements from the oils depending on the complexity and size of their respective organic molecules.

Synthesis

Manganese and Mo are enriched in authigenic pyrite derived from oil seeps compared to pyrite derived from methane seeps. This co-enrichment may be due to a persistent sulphidic environment that is seldom disrupted by pulses of oxygenation due to shifting redox boundaries in the sediment; conditions maintained by the oxidation of crude oil. These conditions would allow for an effective incorporation of Mo into pyrite, while also providing conditions that facilitate Mn uptake by pyrite. The presence of a Mn (oxy)hydroxide shuttle process at oil seeps would also explain the co-enrichment of Mn and Mo in oil seep pyrite. The enrichment of Cu, Zn, and Ni at oil seeps also argues for persistent sulphidic conditions and an additional source of these elements to pore water, both being triggered by the microbial oxidation of crude oil. The presence of an enhanced particulate shuttle process driven by Mn (oxy)hydroxides at oil seeps as invoked above is currently unknown, and represents a yet poorly constrained source for trace elements to bottom waters above seepage environments. Distinguishing the exact sources of trace elements in the two seepage systems that may include crude oil, as well as the dissolution of carbonates and clay minerals in the host sediments, will shed more light on trace element dynamics during early diagenesis. Comparing these results to other seepage sites from more diverse environments will increase the potential of pyrite based trace element proxies.

Acknowledgements

This research was funded by the "Independent Projects for Postdocs" grant scheme awarded to DS by the Central Research Development Fund of the University of Bremen. We thank Anne Hübner, Stefan Sopke, Janice Malnati, and Andreas Klügel (University of Bremen) for sample preparation and assistance in EMPA analyses.

Editor: Juan Liu

Data Availability Statement

Data will be made available on the Pangaea database (www.pangaea.de).

Additional Information

Supplementary Information accompanies this letter at https://www.geochemicalperspectivesletters.org/article2409.

Cite this letter as: Smrzka, D., Lin, Z., Monien, P., Chen, T., Bach, W., Peckmann, J., Bohrmann, G. (2024) Pyrite-based trace

element fingerprints for methane and oil seepage. *Geochem. Persp. Let.* 29, 33–37. https://doi.org/10.7185/geochemlet.2409

References

Akam, S.A., Lyons, T.W., Coffin, R.B., McGee, D., Naehr, T.H., Bates, S.M., Clarkson, C., Reese, B.K. (2021) Carbon-sulfur signals of methane versus crude oil diagenetic decomposition and U-Th age relationships for authigenic carbonates from asphalt seeps, southern Gulf of Mexico. *Chemical Geology* 581, 120395. https://doi.org/10.1016/j.chemgeo.2021.120395

Atienza, N.M.M., Gregory, D.D., Taylor, S.D., Swing, M., Perea, D.E., Owens, J.D., Lyons, T.W. (2023) Refined views of ancient ocean chemistry: Tracking trace element incorporation in pyrite framboids using atom probe tomography. *Geochimica et Cosmochimica Acta* 357, 1–12. https://doi.org/10.1016/j.gca.2023.07.013

Chen, C., Wang, J., Algeo, T.J., Zhu, J.-M., Wang, Z., Ma, X., Cen, Y. (2023) Sulfate-driven anaerobic oxidation of methane inferred from trace-element chemistry and nickel isotopes in pyrite. *Geochimica et Cosmochimica Acta* 349, 81–95. https://doi.org/10.1016/j.gca.2023.04.002

Domingos, J.M., Runge, E., Dreher, C., Chiu, T.-H., Shuster, J., Fischer, S., Kappler, A., Duda, J.-P., Xu, J., Mansor, M. (2023) Inferred pyrite growth via the particle attachment pathway in the presence of trace metals. *Geochemical Perspectives Letters* 26, 14–19. https://doi.org/10.7185/geochemlet.2318

Duyck, C., Miekeley, N., Porto da Silveira, C.L., Aucélio, R.Q., Campos, R.C., Grinberg, P., Brandao, G.P. (2007) The determination of trace elements in crude oil and its heavy fractions by atomic spectrometry. *Spectrochimica Acta Part B* 62, 939–951. https://doi.org/10.1016/j.sab.2007.04.013.

Feng, D., Chen, D., Peckmann, J. (2009). Rare earth elements in seep carbonates as tracers of variable redox conditions at ancient hydrocarbon seeps. *Terra Nova* 21, 49–56. https://doi.org/10.1111/j.1365-3121.2008.00855.x.

Gregory, D.D., Large, R.R., Halpin, J.A., Baturina, E.L., Lyons, T.W., Wu, S., Danyushevsky, L., Sack, P.J., Chappaz, A., Maslennikov, V.V., Bull, S.W. (2015) Trace element content of sedimentary pyrite in black shales. *Economic Geology* 110, 1389–1410. https://doi.org/10.2113/econgeo.110.6.1389

Huerta-Diaz, M.A., Morse, T.W. (1992) Pyritization of trace metals in anoxic marine sediments. *Geochimica et Cosmochimica Acta* 56, 2681–2702. https://doi.org/10.1016/0016-7037(92)90353-K

Joye, S.B., Boetius, A., Orcutt, B.N., Montoya, J.P., Schulz, H.N., Erickson, M.J., Lugo, S.K. (2004) The anaerobic oxidation of methane and sulfate reduction in sediments from Gulf of Mexico cold seeps. *Chemical Geology* 205, 219–238. https://doi.org/10.1016/j.chemgeo.2003.12.019

Krake, N, Birgel, D., Smrzka, D., Zwicker, J., Huang, H., Feng, D., Bohrmann, G., Peckmann, J. (2022) Molecular and isotopic signatures of oil-driven bacterial sulfate reduction at seeps in the southern Gulf of Mexico. *Chemical Geology* 595, 120797. https://doi.org/10.1016/j.chemgeo.2022.120797

Large, R.R., Halpin, J.A., Danyushevsky, L.V., Maslennikov, V.V., Bull, S.W., Long, J.A., Gregory, D.D., Lounejeva, E., Lyons, T.W., Sack, P.J., McGoldrock, P.J., Calver, C.R. (2014) Trace element content of sedimentary pyrite as a new proxy for deep-time ocean-atmosphere evolution. *Earth and Planetary Science Letters* 389, 209–220. https://doi.org/10.1016/j.epsl.2013.12.020

Lin, Z., Sun, X., Chen, K., Strauss, H., Klemd, R., Smrzka, D., Chen, T., Lu, Y., Peckmann, J. (2022) Effects of sulfate reduction processes on the trace element geochemistry of sedimentary pyrite in modern seep environments. *Geochimica et Cosmochimica Acta* 333, 75–94. https://doi.org/10.1016/j.gca.2022.06.026

Miao, X., Feng, X., Li, J., Liu, X., Liang, J., Feng, J., Xiao, Q., Dan, X., Wie, J. (2022) Enrichment mechanism of trace elements in pyrite under methane seepage. *Geochemical Perspectives Letters* 21, 18–22. https://doi.org/10.7185/geochemlet.2211

Morse, J.W., Arakaki, T. (1993) Adsorption and coprecipitation of divalent metals with mackinawite (FeS). *Geochimica et Cosmochimica Acta* 57, 3635–3640. https://doi.org/10.1016/0016-7037(93)90145-M

Morse, J.W., Luther III, G.W. (1999) Chemical influences on trace metal-sulfide interactions in anoxic sediments. *Geochimica et Cosmochimica Acta* 63, 3373–3378. https://doi.org/10.1016/S0016-7037(99)00258-6

Orcutt, B.N., Joye, S.M., Kleindienst, S., Knittel, K., Ramette, A., Reitz, A., Samarkin, V., Treude, T., Boetius, A. (2010) Impact of natural oil and higher hydrocarbons on microbial diversity, distribution, and activity in Gulf of Mexico cold-seep sediments. *Deep-Sea Research II* 57, 2008–2021. https://doi.org/10.1016/j.dsr2.2010.05.014

Sadowski, Z., Szubert, A., Maliszewksa, I., Jazdzyk, E. (2007) A view on the organic matter and metalloporphyrins biodegradation as characteristic components of black shale ores. *Advanced Materials Research* 20-21, 95–98. https://doi.org/10.4028/www.scientific.net/AMR.20-21.95

Sahling, H., Borowski, C., Escobar-Briones, E., Gaytán-Caballero, A., Hsu, C.-W., Loher, M., MacDonald, I., Marcon, Y., Pape, T., Römer, M., Rubin-Blum, M., Schubotz, F., Smrzka, D., Wegener, G., Bohrmann, G. (2016) Massive asphalt deposits, oil seepage, and gas venting support abundant chemosynthetic communities at the Campeche Knolls, southern Gulf of Mexico. *Biogeosciences* 13, 4491–4512. https://doi.org/10.5194/bg-13-4491-2016

Scholz, F., McManus, J., Sommer, S. (2013) The manganese and iron shuttle in a modern euxinic basin and implications for molybdenum cycling at euxinic ocean margins. *Chemical Geology* 355, 56–68. http://dx.doi.org/10.1016/j.chemgeo.2013.07.006

Schubotz, F., Lipp, J.S., Elvert, M., Kasten, S., Prieto Mollar, X., Zabel, M., Bohrmann, G., Hinrichs, K.-U. (2011) Petroleum degradation and associated microbial signatures at the Chapopote asphalt volcano, Southern Gulf of Mexico. *Geochimica et Cosmochimica Acta* 75, 4377–4398. https://doi.org/10.1016/j.gca.2011.05.025

Shikazono, N., Nakata, M., Tokuyama, E. (1994) Pyrite with high Mn content from the Nankai Trough formed from subduction-induced cold seepage. *Marine Geology* 118, 303–313. https://doi.org/10.1016/0025-3227(94)90090-6

Smrzka, D., Zwicker, J., Klügel, A., Monien, P., Bach, W., Bohrmann, G., Peckmann, J. (2016) Establishing criteria to distinguish oil-seep from methane-seep carbonates. *Geology* 44, 667–670. https://doi.org/10.1130/G38029.1

Smrzka, D., Zwicker, J., Misch, D., Walkner, C., Gier, S., Monien, P., Bohrmann, G., Peckmann, J. (2019a) Oil seepage and carbonate formation: A case study from the southern Gulf of Mexico. *Sedimentology* 66, 2318–2353. https://doi.org/10.1111/sed.12593

Smrzka, D., Zwicker, J., Bach, W., Feng, D., Himmler, T., Chen, D., Peckmann, J. (2019b) The behavior of trace elements in seawater, sedimentary pore water, and their incorporation into carbonate minerals: A review. *Facies* 65, article 41. https://doi.org/10.1007/s10347-019-0581-4

Smrzka, D., Feng, D., Himmler, T., Zwicker, J., Hu, Y., Monien, P., Tribovillard, N., Chen, D., Peckmann, J. (2020) Trace elements in methane-seep carbonates: Potentials, limitations, and perspectives. *Earth-Science Reviews* 208, article 103263. https://doi.org/10.1016/j.earscirev.2020.103263

Suess, E. (1978) Mineral phases formed in anoxic sediments by microbial decomposition of organic matter. *Geochimica et Cosmochimica Acta* 43, 339–352. https://doi.org/10.1016/0016-7037(79)90199-6

Thomson, J., Jarvis, I, Green, R.H., Green, D.A., Clayton, T. (1998) Mobility and immobility of redox-sensitive elements in deep-sea turbidites during shallow burial. *Geochimica et Cosmochimica Acta* 62, 643–656. https://doi.org/10.1016/S0016-7037(97)00378-5.

Tissot, B.T., Welte, D.H. (1984) *Petroleum formation and occurrences*. 2nd edition Springer, Berlin.

Tseng, Y., Römer, M., Lin, S., Pape, T., Berndt, C., Chen, T.-T., Paull, C.K., Caress, D.W., Bohrmann, G. (2023) Yam Seep at Four-Way Closure Ridge: a prominent active gas seep system at the accretionary wedge SW offshore Taiwan. *International Journal of Earth Sciences* 112, 1043–1061. https://doi.org/10.1007/s00531-022-02280-4

Wang, B., Lei, H., Huang, F. (2022) Impacts of sulfate-deriven anaerobic oxidation of methane on the morphology, sulfur isotope, and trace element content of authigenic pyrite in marine sediments of the northern South China Sea. *Marine and Petroleum Geology* 139, article 105578. https://doi.org/10.1016/j.marpetgeo.2022.105578

Geochemical Perspectives Letters

Pyrite-based trace element fingerprints for methane and oil seepage

D. Smrzka, Z. Lin, P. Monien, T. Chen, W. Bach, J. Peckmann, G. Bohrmann

Supplementary Information

The Supplementary Information includes:

- Methods
- Results
- Tables S-1 to S-4
- Figures S-1 to S-3

Methods

This supplementary information includes details on pyrite sampling, sample preparation and geochemical analyses. Pyrite was sampled from oil seep sediments at Mictlan Knoll, Tsanyao Yang Knoll and Knoll 2000 (Campeche Knolls, Sahling *et al.,* 2016), as well as from Challenger Knoll (Sigsbee Knolls; Fig. 1a; Sahling and Bohrmann, 2017). Methane seepage-derived pyrite was sampled from cores taken at Four-Way-Closure Ridge (FWCR) offshore Taiwan (Fig. 1b; Tseng *et al*., 2023). The cores were sampled in intervals of 20 cm, each sample containing ca. 30 grams of sediment. Sediment samples were freeze-dried over 24 h, and subsequently powdered by hand using an agate pestle and mortar. The ground sediments were then sieved with deionised water through a 0.063 mm sieve, and pyrite aggregates were hand-picked under a binocular microscope from the coarse fraction. Pyrite grains were mounted onto epoxy discs, polished to a smooth surface and coated with carbon for electron microprobe analysis (EMPA). Scanning electron microscopy (SEM) was conducted using a Zeiss Supra 40 instrument equipped with a Bruker EDX system. All pyrite samples are present as tubular aggregates, which are themselves composed of smaller framboidal clusters and aggregates of pyrite crystals (Fig. S-1). Uncoated discs were used for laser ablation inductively coupled plasma mass spectrometry (LA-ICP-MS). Prior to EMPA and LA-ICP-MS, mounted pyrite was investigated by reflected light microscopy to select suitable samples for further analyses.

Major element composition of pyrite was determined using a Cameca SX-100 electron microprobe at the Faculty of Geosciences, University of Bremen. Analytical conditions included an acceleration voltage of 20 kV, beam current of 20 nA, and a defocussed beam between 1 and 10 µm diameter. Counting times were 20 s on peak and 10 s on background. For quantification natural minerals from the faculty collection and from the Smithsonian Institution (Jarosewich *et al*., 1980), and the built-in PAP matrix correction were used. Spot sizes and locations were chosen in order to account for sample heterogeneity for each sample in order to arrive at a representative average Fe value used for subsequent LA-ICP-MS data quantification.

LA-ICP-MS was conducted using a NewWave UP 193 nm solid-state laser coupled to a Thermo-Finnigan Element 2 HR-ICP-MS at the University of Bremen. The ICP-MS was operated with a plasma power of 1200 W, while helium (He; 0.8 L min-1) was used as a sample gas, and argon (Ar; 0.8 L min^{-1}) was used as carrier gas. A single spot ablation pattern with a laser pulse rate of 5 Hz, an irradiance of approx. 1.3 GW cm^{-2}, and beam diameters of 30 µm were applied. Total analysis time for each spot was 60 s, including 30 s for gas blank analysis. Pre-ablation was conducted with a beam diameter slightly larger than the beam diameter used for the actual measurement. After every 5 to 10 samples NIST610 glass was analysed as external calibration standard using the values of Jochum *et al*. (2011). During laser ablation each sample point was monitored using the time-resolved chromatograms during the measurements in order to discard any sample with irregular or low iron content. The Cetac GeoPro™ software was used for data quantification and ^{56}Fe was used as the internal standard. The NIST610 (USGS) glass standard was used for external calibration for Mn, Zn, Mo, Cd, U and Cu. Due to the lack of sufficient sulfide reference material, data quality was assessed by regular analyses of USGS reference materials BCR-2G, BHVO-2G (basaltic glasses) and MASS-1 sulfide standard (USGS, Wilson *et al*., 2002) along with the samples. Because these glass reference materials are unsuitable for the quantitative analysis of sulfides, a matrix normalisation calibration strategy was applied (Liu *et al*., 2008; Yuan *et al*., 2012). Trace elements in pyrite were analysed by multi-external standards with matrix normalisation and an iron internal standardisation. This calibration method employed a basaltic glass reference material (BHVO-2G) as a transition bridge and multi-glass reference materials with matrix normalisation plus internal standardisation (Fe as the internal standard) to determine the trace elemental composition of sulfide minerals (cf. Yuan *et al*., 2012; Miao *et al*., 2022). The MASS-1 reference material was used as a secondary independent control standard given that the silicate glass reference materials are not well suited for analysis if used alone. The analytical results of trace elements obtained by multi-external standards with matrix normalisation plus Fe internal standardisation show relative standard deviations (RSD) below 10 % except for Zn, as well as relative errors better than 10 % for all measured elements except for Mo and Zn (Table S-2).

Trace element composition of bulk sediments was conducted using an Agilent Technologies 7700x quadrupole ICP-MS at Nanjing FocuMS Technology Co. Ltd. About 40 mg powder was transferred into high-pressure PTFE bombs mixed with 0.5 ml 60 wt. % HNO_3 and 1.0 ml 40 % HF. These bombs were sealed and placed in the oven at 195 ℃ for 72 hours to ensure complete digestion. After cooling, the bombs were opened, dried down on a hotplate, treated with 5 ml 15 wt. % HNO_3 and 1ml Rh internal standard, then sealed and placed in the oven at 150 ℃ overnight. Then Aliquot of the digestions were diluted 2000-fold and nebulised into ICP-MS to determine trace elements. Geochemical reference materials of basalt (BHVO-2) and andesite (AGV-2) were used as quality control. Deviation was better than 10 % for all measured elements.

Results

There is no evidence for hydrothermalism in both study areas (MacDonald *et al*., 2004; Sahling *et al*., 2016; Tseng *et al*., 2023), and can therefore be ruled out as a potential source for trace element enrichment to the sediments and pyrites. Trace element geochemistry shows that Mn/Fe *vs.* Mo distributions in pyrite and bulk sediments show similar distribution patterns (Fig. S-2a). Zinc is enriched in methane seep sediments, whereas Cu is enriched in oil seep sediments (Fig. S-2b). Also, Ni is more significantly enriched in these latter sediments than in pyrite (Fig. S-2c). The content of detrital elements Al and Ti in sediments from the South China Sea sites is, on average, higher than in the Gulf of Mexico oil seep sediments (Fig. S-2d-f). Further, there is no correlation between Mn and Al in the sediments (Fig. S-2d), suggesting that Mn is not derived from detrital alumosilicate material.

This suggests the following:

1. Alumosilicates are not responsible for Mn, Mo, Zn, Cu, Ni, and V enrichments in pyrite. Moreover, Mn shows no correlation to Al in the sediment, indicating that its enrichment is authigenic.
2. Manganese and Mo enrichment at oil seeps is authigenic, in the pyrite and the sediments, being most likely associated with the presence and oxidation of oil in the sediments as outlined in in the discussion chapter “A combined Fe-Mn-Mo fingerprint” in the main article.

3. Copper and Zn show different patterns in the sediment, suggesting that these elements are enriched by an authigenic process in pyrite as outlined in the discussion chapter "A combined Cu-Zn-Ni-V fingerprint" (main article)., and that they have high affinities for pyrite incorporation.
4. Nickel is enriched in oil seep sediments, probably due to the presence of oil and the high Ni content of oils (cf. Smrzka *et al*., 2019).

We have added a bar plot (Fig. S-3) showing calculated enrichment factors (EFs) of the host sediments (EF = (EL/Alsample)/(EL/Alshale)).

Supplementary Tables

Tables S-1 to S-4 are available for download (Excel) from the online version of this article at https://doi.org/10.7185/geochemlet.2409

Table S-1 Major and trace elemental composition of pyrite derived from oil- and methane-dominated seeps, all values in ppm. All data acquired by LA-ICP-MS except for Fe, which was determined via EMPA.

Table S-2 Precision and accuracy of determined major and trace elements in pyrite shown in Table S-1.

Table S-3 Trace element geochemistry of sediment cores.

Table S-4 Calculated sediment trace element enrichment factors.

Supplementary Figures

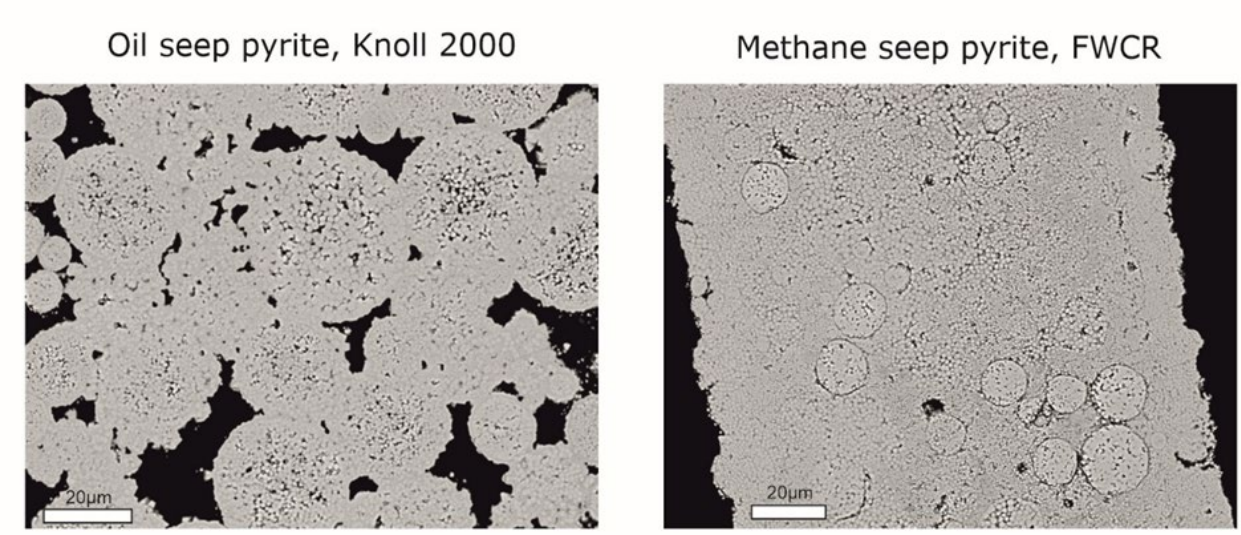

Figure S-1 SEM images of authigenic pyrite from oil and methane seep sediments.

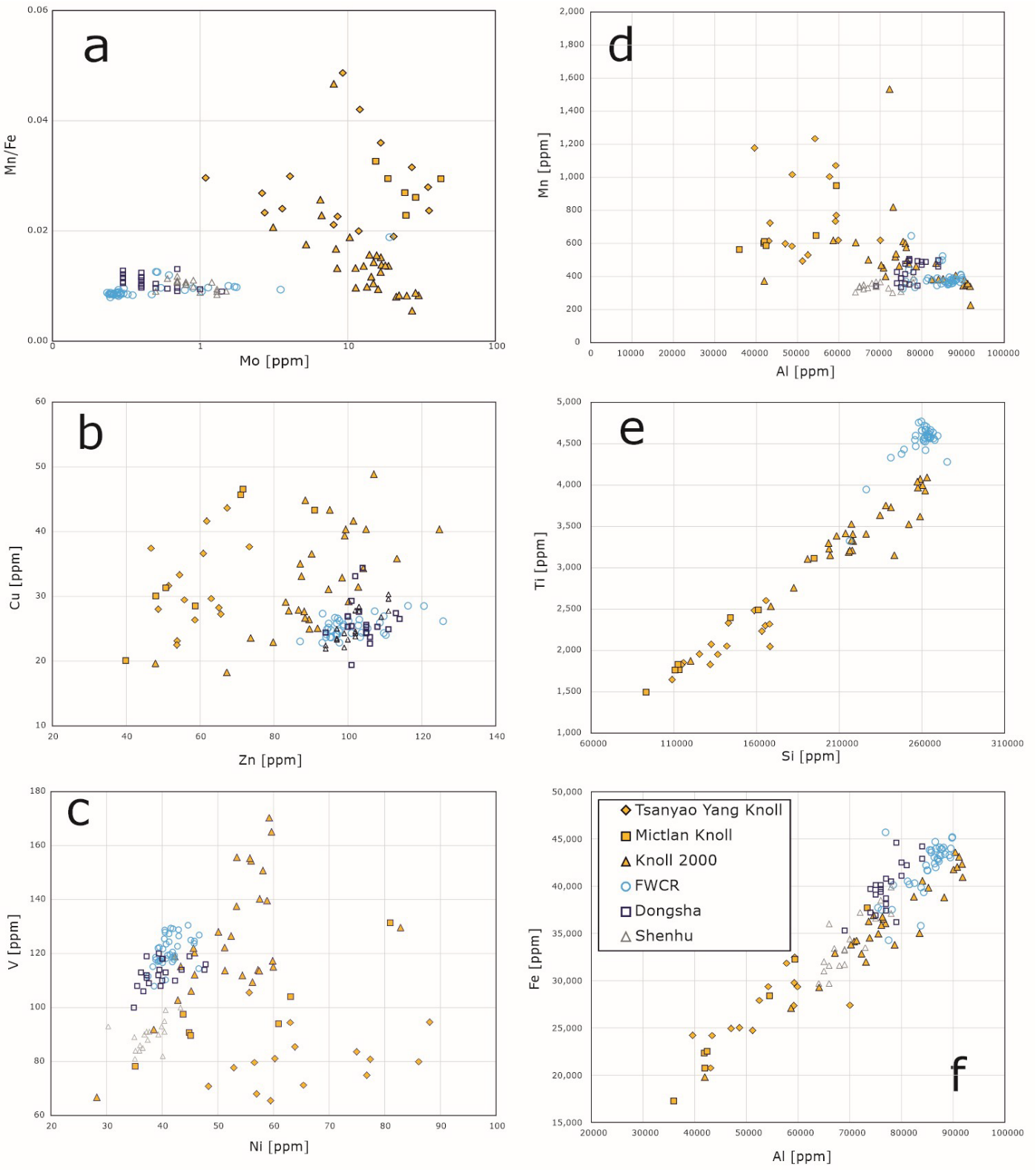

Figure S-2 Trace element distribution in oil- and methane-seep sediments.

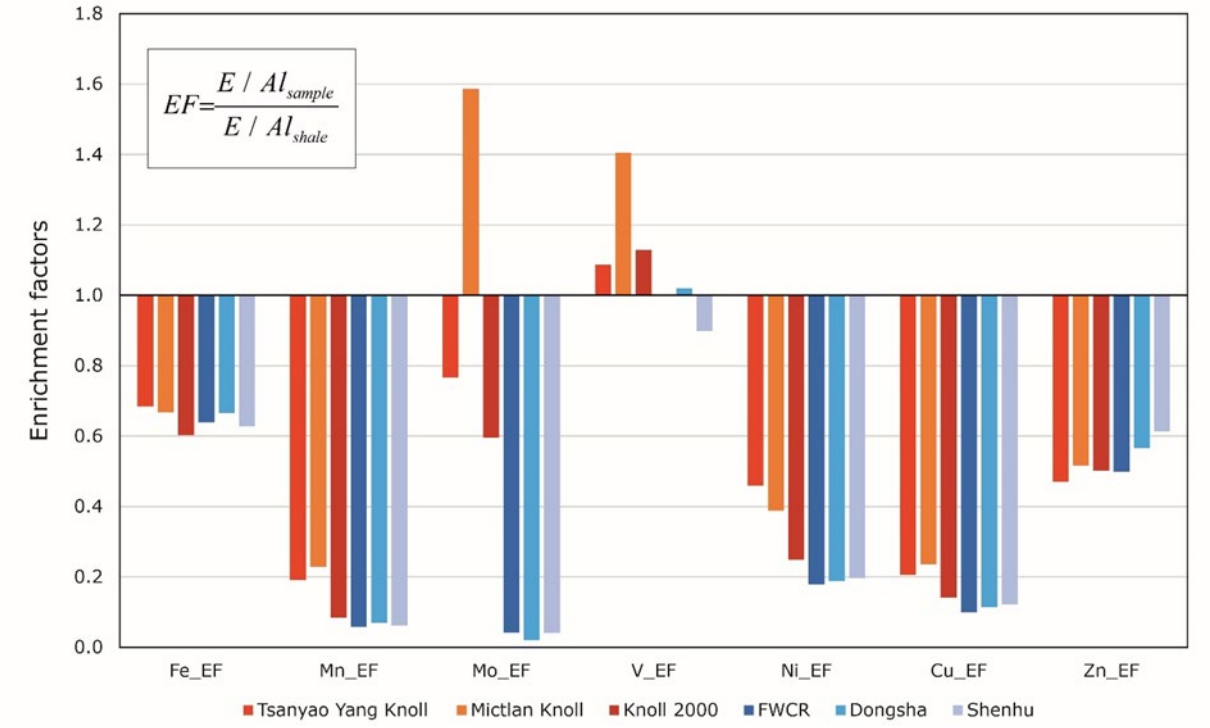

Figure S-3 Calculated trace element enrichment factors (EFs) in oil- and methane-seep sediments.

Supplementary Information References

Jarosewich, E., Nelen, J.A., Norberg, J.A. (1980) Reference samples for electron microprobe analysis. *Geostandards Newsletter* 4, 43-47. https://doi.org/10.1111/j.1751-908X.1980.tb00273.x.

Jochum, K.P., Weis, U., Stoll, B., Kuzmin, D., Yang, Q., Raczek, I., Jacob, D.E., Stracke, A., Birbaum, K., Frick, D.A., Günther, D., Enzweiler, J. (2011) Determination of reference values for NIST SRM 610-617 glasses following ISO guidelines. *Geostandards and Geoanalytical Research* 35, 397-429. https://doi.org/10.1111/j.1751-908X.2011.00120.x.

Liu, Y., Hu, Y., Gao, S., Günther, D., Xu, J., Gao, C., Chen, H. (2008) *In situ* analysis of major and trace elements of anhydrous minerals by LA-ICP-MS without applying an internal standard. *Chemical Geology* 257, 34-43. https://doi.org/10.1016/j.chemgeo.2008.08.004.

MacDonald, I.R., Bohrmann, G., Escobar, E., Abegg, F., Blanchon, P., Blinova, V., Brückmann, W., Drews, M., Eisenhauer, A., Han, X., Heeschen, K., Meier, F., Mortera, C., Naehr, T., Orcutt, B., Bernard, B., Brooks, J., De Faragó, M. (2004) Asphalt Volcanism and Chemosynthetic Life in the Campeche Knolls, Gulf of Mexico. *Science* 304, 999-1002. https://doi.org/10.1126/science.1097154.

Miao, X., Feng, X., Li, J., Liu, X., Liang, J., Feng, J., Xiao, Q., Dan, X., Wie, J. (2022) Enrichment mechanism of trace elements in pyrite under methane seepage. *Geochemical Perspectives Letters* 21, 18-22. https://doi.org/10.7185/geochemlet.2211.

Sahling, H., Bohrmann, G., Cruise Participants (2017) R/V METEOR Cruise Report M114, Natural hydrocarbon seepage in the southern Gulf of Mexico, Kingston - Kingston, 12 February - 28 March 2015. Berichte, MARUM–Zentrum für Marine Umweltwissenschaften, Fachbereich Geowissenschaften, Universität Bremen 315, 1–214. urn:nbn:de:gbv:46-00105897-18.

Sahling, H., Borowski, C., Escobar-Briones, E., Gaytán-Caballero, A., Hsu, C.-W., Loher, M., MacDonald, I., Marcon, Y., Pape, T., Römer, M., Rubin-Blum, M., Schubotz, F., Smrzka, D., Wegener, G., Bohrmann, G. (2016) Massive asphalt deposits, oil seepage, and gas venting support abundant chemosynthetic communities at the Campeche Knolls, southern Gulf of Mexico. *Biogeosciences* 13, 4491-4512. https://doi.org/10.5194/bg-13-4491-2016.

Tseng, Y., Römer, M., Lin, S., Pape, T., Berndt, C., Chen, T.-T., Paull, C.K., Caress, D.W., Bohrmann, G. (2023) Yam Seep at Four-Way Closure Ridge: a prominent active gas seep system at the accretionary wedge SW offshore Taiwan. *International Journal of Earth Sciences* 112, 1043-1061. https://doi.org/10.1007/s00531-022-02280-4.

Wilson, S.A., Ridley, W.I., Koenig, A.E. (2002) Development of sulfide calibration standards for the laser ablation inductively-coupled plasma mass spectrometry technique. *Journal of Analytical Atomic Spectrometry* 17, 406-409. https://doi.org/10.1039/B108787H.

Yuan, J.-H., Zhan, X.-C., Fan, C.-Z., Zhao, L.-H., Sun, D.-Y., Jia, Z.-R., Hu, M.-Y., Kuai, L.-J. (2012) Quantitative analysis of sulfide minerals by laser ablation-inductively coupled plasma-mass spectrometry using glass reference materials with matrix normalization plus sulfur internal standardization calibration. *Chinese Journal of Analytical Chemistry* 40, 201-207. https://doi.org/10.1016/S1872-2040(11)60528-8.